Biomineralization control related to population density under ocean acidification

Stefano Goffredo[1]*, Fiorella Prada[1], Erik Caroselli[1], Bruno Capaccioni[2], Francesco Zaccanti[1], Luca Pasquini[3], Paola Fantazzini[3,4], Simona Fermani[5], Michela Reggi[5], Oren Levy[6], Katharina E. Fabricius[7], Zvy Dubinsky[6] and Giuseppe Falini[5]*

Anthropogenic CO_2 is a major driver of present environmental change in most ecosystems[1], and the related ocean acidification is threatening marine biota[2]. With increasing $p\mathrm{CO_2}$, calcification rates of several species decrease[3], although cases of upregulation are observed[4]. Here, we show that biological control over mineralization relates to species abundance along a natural pH gradient. As $p\mathrm{CO_2}$ increased, the mineralogy of a scleractinian coral (_Balanophyllia europaea_) and a mollusc (_Vermetus triqueter_) did not change. In contrast, two calcifying algae (_Padina pavonica_ and _Acetabularia acetabulum_) reduced and changed mineralization with increasing $p\mathrm{CO_2}$, from aragonite to the less soluble calcium sulphates and whewellite, respectively. As $p\mathrm{CO_2}$ increased, the coral and mollusc abundance was severely reduced, with both species disappearing at pH < 7.8. Conversely, the two calcifying and a non-calcifying algae (_Lobophora variegata_) showed less severe or no reductions with increasing $p\mathrm{CO_2}$, and were all found at the lowest pH site. The mineralization response to decreasing pH suggests a link with the degree of control over the biomineralization process by the organism, as only species with lower control managed to thrive in the lowest pH.

Several studies on the influence of pH on crystallography and texture of calcified regions are _ex situ_, short-term experiments on isolated organisms[5], providing important information, but unrepresentative of natural ecosystems and failing to assess long-term effects[6]. There is a great need for long-term analyses on ocean acidification effects on marine ecosystems acclimated to high $p\mathrm{CO_2}$, as found around CO_2 vents. Vents are not perfect predictors of future oceans, owing to pH variability, proximity of unaffected populations, and co-varying environmental parameters[7]. However, vents acidify sea water on sufficiently large temporal and spatial scales to integrate ecosystem processes[6], acting as 'natural laboratories'. In Papua New Guinea vents, reductions in coral diversity, recruitment and abundance, and shifts in competitive interactions, are found[8]. In Mediterranean vents, decreased diversity, biomass, trophic complexity and abundance in many calcifying and non-calcifying organisms, and increases in macroalgae and seagrasses, are observed[7,9,10].

We assessed, along a natural pH gradient, the effect of $p\mathrm{CO_2}$ on the mineralization and abundances of the aragonitic scleractinian

B. europaea, the aragonitic tube-forming gastropod _V. triqueter_, the brown alga _P. pavonica_, which deposits aragonite on the thalli surface, the green alga _A. acetabulum_, whose cups' outer surfaces are calcified with aragonite and a small amount of whewellite (calcium oxalate), and the non-mineralized brown alga _L. variegata_. The mineralization is biologically controlled in _V. triqueter_ (that is, mineral is deposited in confined nucleation sites under complete biological control with minimal environmental effects), biologically induced in _P. pavonica_ and _A. acetabulum_ (that is, it is strongly affected by the environment with minimal biological control), whereas _B. europaea_ may represent an intermediate and still controversial situation[11]. We aimed to assess changes in the mineralization and abundance of species along a $p\mathrm{CO_2}$ gradient in relation to their control over biomineralization.

Mean pH, CO_2, saturation of calcite (Ω_{calc}), and of aragonite (Ω_{arag}) differed among Sites (Kruskal–Wallis test/analysis of variance, $p < 0.001$). The median pH values were 8.1 (Site 1), 7.9 (Site 2), 7.8 (Site 3) and 7.7 (Site 4), with increasing variability towards Site 4 (Fig. 1 and Supplementary Fig. 1 and Table 1).

Aragonite was the only mineral phase in _B. europaea_ skeletons (Supplementary Fig. 2). Organic matrix content was homogeneous among Sites (Kruskal–Wallis test, $p > 0.05$; Supplementary Fig. 3 and Table 1). Skeletal texture exhibited fibres evolving from a centre of calcification (Supplementary Fig. 4), but the morphology of these centres, and fibre thickness ($600 \pm 200\,\mathrm{nm}$), were not related to $p\mathrm{CO_2}$ (Supplementary Fig. 5). Hardness was homogeneous among sample regions and study Sites ($5100 \pm 600\,\mathrm{MPa}$). The elastic Young's modulus decreased (that is, the skeleton became less stiff) along the aboral to oral direction and was lower at Sites 2 and 3 than at Site 1 (Supplementary Table 2). Crystal quality and fibre thickness usually increases when crystallization occurs under lower supersaturation[12]. Although a reduction of precipitation rate with $p\mathrm{CO_2}$ could increase crystal quality, other mechanisms could involve organic matrix molecules. Corals seem to maintain a high pH at the nucleation sites within the calicoblastic layer, possibly expending a significant amount of energy[13]. This is supported by the lack of increase in aragonite fibre thickness with decreasing seawater Ω_{arag}, which would be expected if Ω_{arag} of the calcification site decreased[12]. The reduction of skeletal stiffness with declining pH is probably associated with an increase in porosity, as confirmed by preliminary
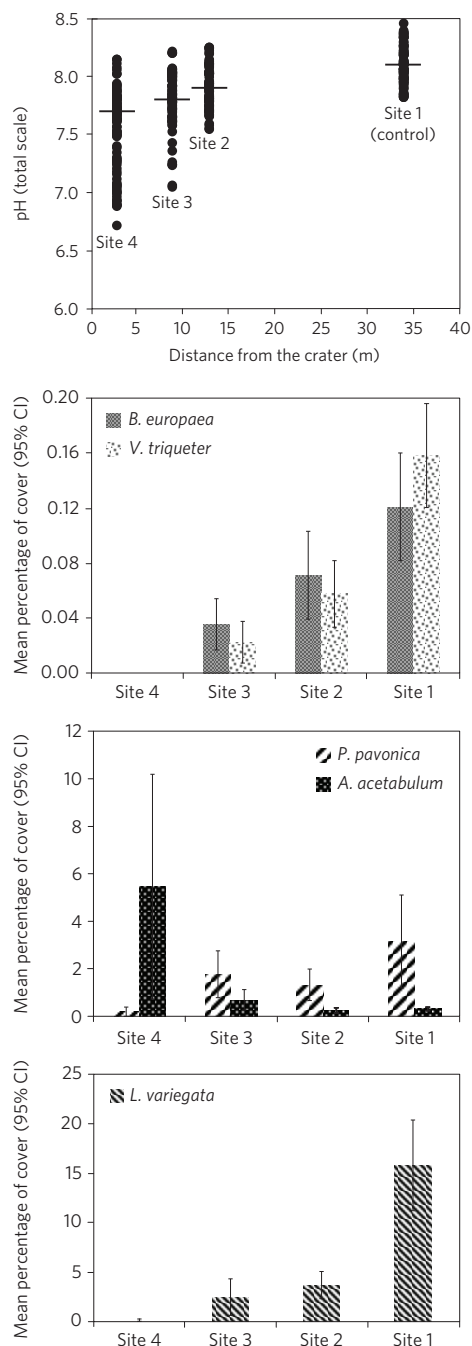
Figure 1 | Range in pH total scale and mean percentage of cover for *Balanophyllia europaea*, *Vermetus triqueter*, *Padina pavonica*, *Acetabularia acetabulum* and *Lobophora variegata* along the pCO_2 gradient. pH measures were 103–110 per site. Horizontal bars indicate the median pH. Error bars are 95% confidence intervals (CI).

nuclear magnetic resonance analyses. *B. europaea* skeletons have already been found to increase their porosity in stress conditions, such as increasing temperature[14].

The apical regions of *V. triqueter* shell-tubes of similar diameter (~5 mm) were analysed. Aragonite was the only mineral phase (Supplementary Fig. 2). Shell-tubes from Site 1 had four layers with different crystal texture and variable relative thickness among samples (Fig. 2). The first two layers were prismatic, with the second one made of regular prisms with a square section (500 nm side). The third was cross-lamellar with regular fibres 500 nm thick. The fourth external layer was spherulitic, with several bores and

channels (Fig. 2). In one of six samples from Site 2, and in four of six from Site 3, the two internal layers were not present. Different hardnesses and elastic Young's moduli were associated with different textures, without significant variations among Sites (Supplementary Table 2). Organic matrix content was homogeneous among Sites (Kruskal–Wallis test, $p > 0.05$; Table 1 and Supplementary Fig. 3). The unaffected mineralogy of *V. triqueter* shell-tubes is possibly due to the exquisite control of biological macromolecules on mollusc mineralization, which occurs in confined sites resulting in complex crystalline textures (Fig. 2). During shell-tube growth, the external layers are the first to be deposited, followed by the internal ones[11]. A pH reduction can reduce the growth rates (calcification) of mollusc shells[15], which probably explains the absence of the internal layers in shell-tubes from the most acidic Sites.

Padina pavonica thallus tips from Site 1 were mainly aragonitic with traces of hydrate calcium sulphate salts (CSh). Aragonite concentration decreased with increasing pCO_2, and almost only CSh was observed at Site 4 (Supplementary Fig. 2). The presence of CSh was investigated in detail by further tests and considerations (Supplementary Information). The overall mineral content differed among Sites (Kruskal–Wallis test, $p < 0.05$; Table 1 and Supplementary Fig. 3), and declined with increasing pCO_2 (Spearman's rho of the correlation with pH = 0.592, $p < 0.01$). In all samples, many aragonite needle-like crystals were aggregated or merged forming bundles. CSh crystals appeared as prisms or tablets (Fig. 3 and Supplementary Fig. 6). The decalcification left the thalli free of mineral deposits (Supplementary Fig. 6). In *P. pavonica*, CSh increased with increasing pCO_2. Some stabilization of CSh salts by algal molecules[16,17], probably polysaccharides, is expected, as in sea water CSh converts to gypsum.

Acetabularia acetabulum was mainly aragonitic, with minor presence of whewellite (Supplementary Fig. 2). All samples contained about 10% (w/w) of water. The content of mineral phases, estimated after pyrolysis and release of water, differed among Sites (Kruskal–Wallis test, $p < 0.01$; Table 1 and Supplementary Fig. 3) and declined with increasing pCO_2 (Spearman's rho of the correlation with pH = 0.555, $p < 0.01$). The aragonite/whewellite ratio decreased with increasing pCO_2. Globular granules of amorphous material rich in Ca and S were observed on the surface of needle-like aragonite aggregates at Sites 1–4 (Fig. 3 and Supplementary Fig. 6). Whewellite was the only phase detected at Site 4 (Fig. 3 and Supplementary Fig. 2), where it appeared as prisms. After decalcification, the cup surface was free of mineral deposits (Supplementary Fig. 6). In line with a mainly chemical mineralization control[17], increasing pCO_2 did not affect deposition of whewellite in *A. acetabulum*. The persistence of amorphous globular particles rich in calcium and sulphur was unexpectedly observed when aragonite disappeared. This phase, soluble in acetic acid solution, may be the result of interactions between Ca ions and the sulphonated groups of polysaccharides.

Within each sample, *P. pavonica* and *A. acetabulum* showed a marked reduction of mineralized areas with increasing pCO_2 (Fig. 4). Their aragonite content decreased with decreasing Ω_{arag}. At a Ω_{arag} of 1.5, aragonite was not observed, probably because this saturation level is too low to sustain its nucleation process. The observed changes in morphology of aragonite crystals (Fig. 3) are associated with seawater chemistry[18].

The percentage of cover for all species, except *A. acetabulum*, differed among Sites (Kruskal–Wallis test, $p < 0.001$), and decreased with increasing pCO_2 (Supplementary Table 3). *B. europaea* and *V. triqueter* were not found at Site 4 (pH = 7.7, Ω_{arag} = 1.5; Fig. 1). Densities of *A. acetabulum* were homogeneous among Sites (Kruskal–Wallis test, $p > 0.05$). This suggests that *P. pavonica* and *A. acetabulum* are not obligate calcifiers, persisting in high pCO_2 where also the non-calcifying species *L. variegata* survives (Fig. 1).

Table 1 | Summary of the main effects of ocean acidification on the mineral distribution and content in the calcified organisms with increasing proximity to the CO_2 seep (declining pH).

			Balanophyllia europaea		Vermetus triqueter		Padina pavonica		Acetabularia acetabulum	
	Median pH	Median Ω_{arag}	Mineral phase	Mineral phase (%)†	Min phase	Mineral phase (%)†	Mineral phases	Mineral phases (%)	Mineral phases*	Mineral phases (%)
Site 1	8.1	3.6	A	97.4 ± 0.4	A	98.0 ± 0.5	A CSh‡	73.9 ± 8.3	A Wh	42.9 ± 3.9
Site 2	7.9	2.4	A	97.80 ± 0.04	A	98.3 ± 0.2	A CSh	71.5 ± 10.6	A Wh	24.2 ± 6.9
Site 3	7.8	2.1	A	97.8 ± 0.2	A	98.1 ± 0.1	A **CSh**	59.6 ± 4.9	A **Wh**	22.7 ± 7.6
Site 4	7.7	1.5	-	-	-	-	A‡ **CSh**	61.6 ± 4.5	Wh	25.4 ± 8.0

Uncertainties are one standard deviation. A, Wh and CSh indicate aragonite, whewellite and monohydrate calcium sulphate salts. The percentage of mineral phase(s) is reported as mass ratio. *Amorphous globular particles were also detected. †The content of organic matrix is the complement to 100 in *B. europaea* and *V. triqueter* where no significant amounts of water were detected in the skeletons and shell-tubes. *P. pavonica* and *A. acetabulum* contained a significant amount of bounded water and their percentage of organic matrix significantly increased with pCO_2. ‡This phase was detected in traces. When two phases were present, the most abundant one is indicated in bold.
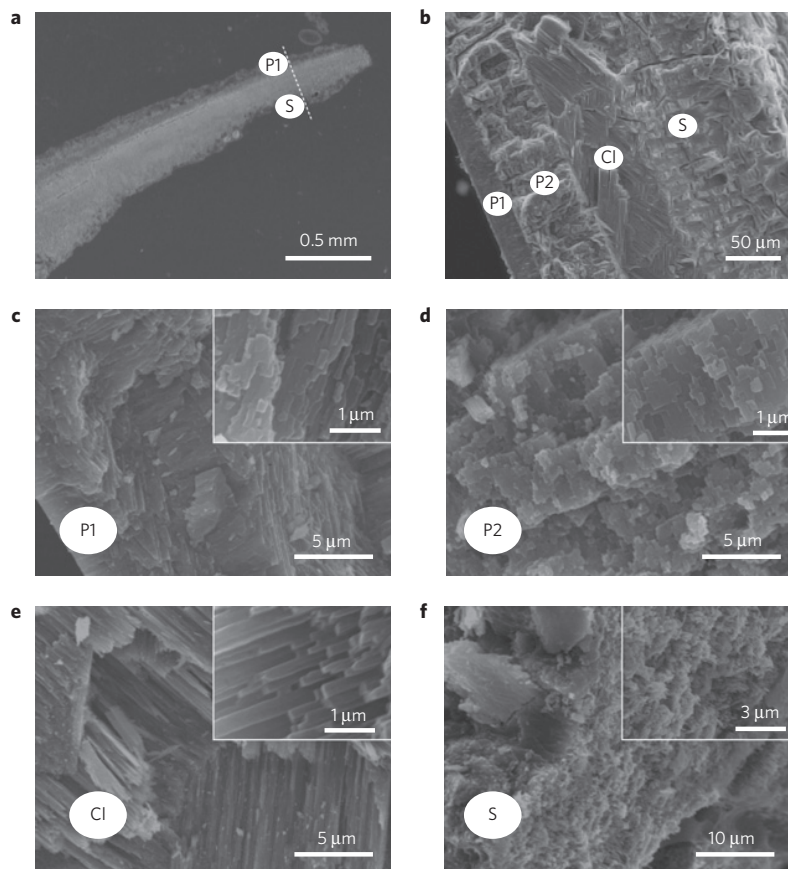
Figure 2 | Scanning electron microscope images of a longitudinal section of *Vermetus triqueter* shell-tube. a, Apical region of shell-tube. High-magnification images were taken along the dotted line from inside (P1) to outside (S) the tube. **b**, Shell-tubes in Site 1 consisted of four layers (P1, P2, Cl, S). **c**, First prismatic layer (P1). **d**, Second prismatic layer (P2), with square cross-sections. **e**, Cross-lamellar layer (Cl). **f**, Spherulitic layer (S) containing bores and channels. The first two layers were not present in one sample from Site 2 and in most of the samples from Site 3.

A changing benthic community was associated with the pCO_2 gradient (Supplementary Video). The coverage of a coral, a mollusc, and two macroalgae, one of which is a calcifier, declined with increasing pCO_2 (Fig. 1). This is in agreement with previous investigations at CO_2 vents, documenting marked reductions in calcifying macroalgal abundance[7,8]. Calcifying organisms seem the most sensitive to elevated pCO_2 (ref. 19), even if their response is not consistent[8,15,20]. *A. acetabulum*, *B. europaea* and *V. triqueter* were previously found only outside vent areas, at a pH_{TS} of 8.14 (ref. 7). Instead, in our survey *B. europaea* and *V. triqueter* survived up to pH_{TS} 7.8 and algal species up to pH_{TS} 7.7 (Fig. 1). The response of macroalgae to pCO_2 is expected to vary among species. As an example, increased cover with decreasing pH was observed for *Padina* spp. at CO_2 seeps in Vulcano and Papua New Guinea[21], and for *L. variegata* at CO_2 seeps in Ischia[10], which contrasts with our data. The response of non-calcifying macroalgae to elevated pCO_2 is variable[22], depending on energy availability[23]. The nature of CO_2-induced shifts in macroalgal community structure is likely to vary depending on other environmental factors, such as nutrient availability, temperature and solar radiation[24]. For instance, *L. variegata* were sampled in Ischia at 1 m depth and in our study at 8–12 m. Growth of the brown alga *Dictyota ciliolata* decreases with decreasing light intensity[25]. In the brown alga *Fucus vesiculosus*, photosynthesis and growth decrease with increasing depth[26] from
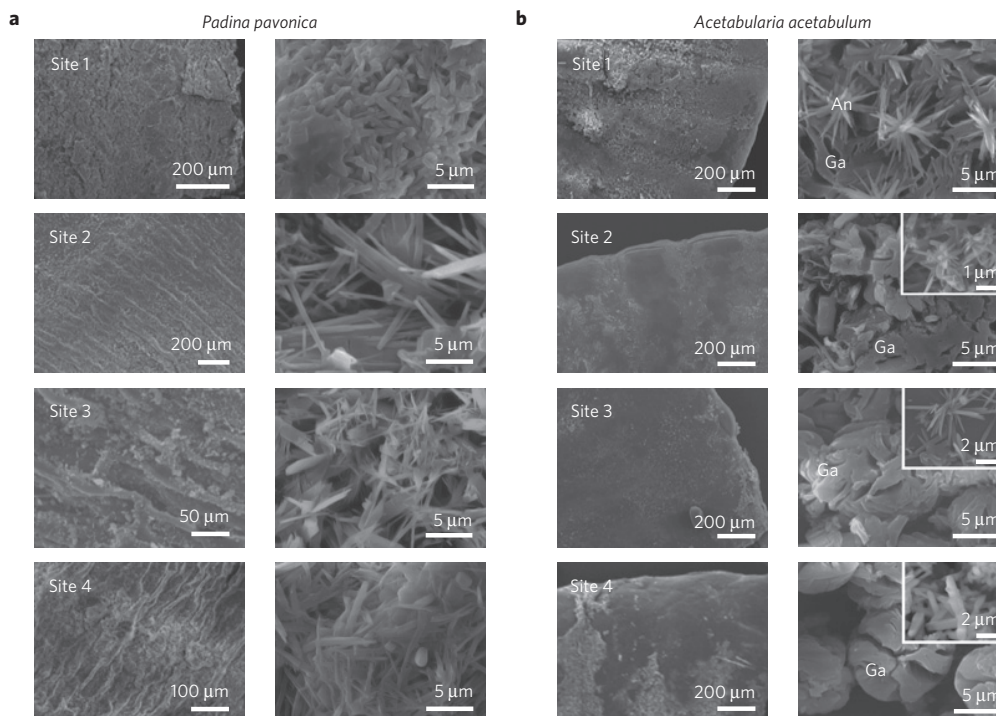
Figure 3 | Scanning electron microscope images of *Padina pavonica* thalli and *Acetabularia acetabulum* cups. a,b, Low-magnification (left column) and high-magnification (right column) images. *P. pavonica* (**a**) became less mineralized with increasing pCO_2. The aggregation and shape of aragonite crystals was lightly affected by pCO_2. In *A. acetabulum* (**b**), needle-like crystals of aragonite (An) were above and among the globular aggregates (Ga). The amount of biomineralized material was reduced with increasing pCO_2, whereas the centre of the cup became more populated by spherical aggregates. Aragonite needles are shown in the inset for Site 2 and 3, and whewellite is shown in the inset for Site 4.

1 to 6 m. At the high light of the shallow Ischia site, *L. variegata* may compensate for the negative effect of lowered pH through enhanced growth.

We related the biological control over biomineralization with changes in the abundance of organisms along natural pCO_2 gradients. The content of biomineralized products decreased with increasing pCO_2 only in the two calcifying algal species (with a weak control over their biomineralization), but the two species with

Figure 4 | *In situ* pictures of *Padina pavonica* and *Acetabularia acetabulum* at Sites 1 and 4, showing the reduction of calcified material (white areas) with increasing pCO_2. A ruler is included in each image to show scale. The smallest tick marks indicate a length of 1 mm.

stronger biomineralization control (*B. europaea* and *V. triqueter*) tolerated less severe pCO_2 increases (pH 7.8) than the algae (pH $\leq$ 7.7). Moreover, the more tolerant algae continued to grow despite their biomineralization products being profoundly altered by pCO_2. Even if biomineralization in algae is only induced[17], we cannot exclude that the switch from aragonite to other biominerals may represent a phenomenon of phenotypic plasticity[27], which is increasingly being found to strongly contribute to persistence in the face of climate change[28]. The control over biomineralization may not be the only cause of the observed differences, because the coral and the mollusc have a biology completely dependent on calcification, whereas the algae do not. Moreover, the algae may benefit from pCO_2 increase in terms of photosynthesis, whereas the coral may be less dependent on the photosynthetic process and the mollusc does not photosynthesize. This study adds new evidence to field studies on ocean acidification effects[4,9,29,30], all indicating major ecological shifts as CO_2 rises. It documented that the mineralization response to ocean acidification seems connected with the organisms' control of biomineralization, increasing pCO_2 profoundly affects the abundance of many benthic organisms, and only the species with weaker control were observed at the lowest pH.

Methods

Study site. Fieldwork was conducted at Panarea, Italy (Supplementary Video and Fig. 1), where hydrothermally stable CO_2 emissions acidify sea water, generating a pH gradient (see Supplementary Information for details).

Carbonate chemistry. Four sampling Sites were selected (Fig. 1 and Supplementary Fig. 1): a control site (Site 1), two intermediate pCO_2 sites (Site 2 and Site 3), and a high pCO_2 site (Site 4). pH (NBS scale), temperature and salinity were measured at each Site during several surveys between July 2010 and May 2013 with a multi-parametric probe (600R, YSI Incorporated) powered from a small boat and operated by SCUBA divers. Bottom-water samples for determination of total alkalinity were collected and analysed using standard methods
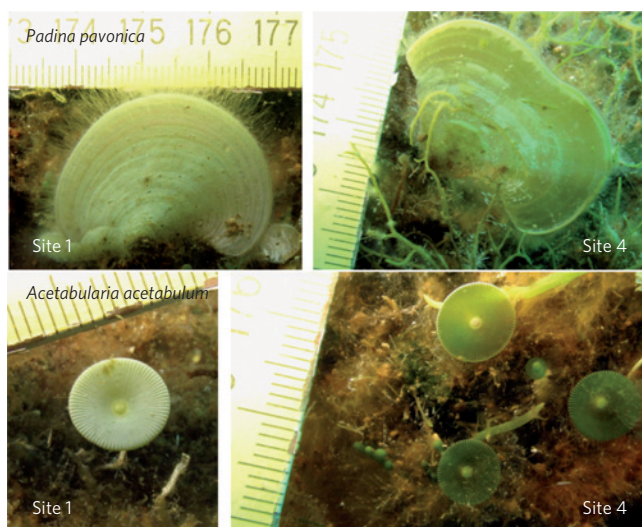
(see Supplementary Information for details). Further temperature data were recorded every three hours by sensors (Thermochron iButton, DS1921G, Maxim Integrated Products) attached in each Site from July 2010 to May 2013. Measured pH was converted to the total scale using CO2SYS software. Median pH (back-transformed hydrogen ion concentrations) were calculated for each Site. The pH, total alkalinity, salinity and temperature were used to calculate other carbonate system parameters using the software CO2SYS (Supplementary Information).

Benthic survey. Photographs of benthos (5 to 10 per Site, 50×50 cm for the animals, 21.0×29.7 cm for the algae) were used to measure the percentage of cover for *B. europaea*, *V. triquetra*, *P. pavonica*, *A. acetabulum* and *L. variegata* at each Site. See Supplementary Information for details.

Vent gas. Gas was sampled during five surveys (June 2011–May 2013) and analysed at the Laboratory of Fluid and Rock Geochemistry of the University of Florence using standard methods (Supplementary Information). Water samples were collected and tested for dissolved H_2S (Supplementary Information).

Statistical analyses. Analysis of variance and the *post hoc* Fisher least significant difference test were used to test for differences among Sites using arcsine and log-transformation for percentage of cover and environmental data, respectively, when necessary. Otherwise, the non-parametric Kruskal–Wallis and Spearman's rank correlation coefficients were used. All analyses were performed using SPSS v.20.

Biomineralization. Samples were randomly collected by SCUBA divers at all Sites and were prepared for analyses with standard methods (Supplementary Information). Microscopic observations and mechanical and spectroscopic measurements required the preparation of cross-sections of the samples (Supplementary Information). X-ray powder diffraction and Fourier transform infrared spectroscopy patterns on small amounts of powdered samples were collected using standard methods (Supplementary Information). Attenuated total reflection Fourier transform infrared spectra of sample cross-sections were acquired with standard methods (Supplementary Information). The organic matter content in the sample was determined by thermogravimetric analysis (Supplementary Information). Microstructures were observed using optical and scanning electronic microscopes (SEM; Supplementary Information). The mechanical properties of shell-tubes and skeletons were measured with standard nano-indentation techniques (Supplementary Information).

References

1. IPCC, *IPCC Special Report on Renewable Energy Sources and Climate Change Mitigation* (Cambridge Univ. Press, 2011).
2. Orr, J. C. *et al.* Anthropogenic ocean acidification over the twenty-first century and its impact on calcifying organisms. *Nature* **437**, 681–686 (2005).
3. Fabry, V. J., Seibel, B. A., Feely, R. A. & Orr, J. C. Impacts of ocean acidification on marine fauna and ecosystem processes. *ICES J. Mar. Sci.* **65**, 414–432 (2008).
4. Rodolfo-Metalpa, R., Martin, S., Ferrier-Pages, C. & Gattuso, J. P. Response of Mediterranean corals to ocean acidification. *Biogeosciences Discuss.* **6**, 7103–7131 (2010).
5. Hahn, S. *et al.* Marine bivalve shell geochemistry and ultrastructure from modern low pH environments: environmental effect versus experimental bias. *Biogeosciences* **9**, 1897–1914 (2012).
6. Barry, J. P., Hall-Spencer, J. M. & Tyrrell, T. Guide to Best Practices for Ocean Acidification Research and Data Reporting (Publications Office of the European Union, 2010).
7. Hall-Spencer, J. M. *et al.* Volcanic carbon dioxide vents show ecosystem effects of ocean acidification. *Nature* **454**, 96–99 (2008).
8. Fabricius, K. E. *et al.* Losers and winners in coral reefs acclimatized to elevated carbon dioxide concentrations. *Nature Clim. Change* **1**, 165–169 (2011).
9. Cigliano, M., Gambi, M. C., Rodolfo-Metalpa, R., Patti, F. P. & Hall-Spencer, J. M. Effects of ocean acidification on invertebrate settlement at volcanic CO_2 vents. *Mar. Biol.* **157**, 2489–2502 (2010).
10. Porzio, L., Buia, M. C. & Hall-Spencer, J. M. Effects of ocean acidification on macroalgal communities. *J. Exp. Mar. Biol. Ecol.* **400**, 278–287 (2011).
11. Lowenstam, H. A. & Weiner, S. *On Biomineralization* (Oxford Univ. Press, 1989).
12. Holcomb, M., Cohen, A. L., Gabitov, R. I. & Hutter, J. L. Compositional and morphological features of aragonite precipitated experimentally from seawater and biogenically by corals. *Geochim. Cosmochim. Acta* **73**, 4166–4179 (2009).
13. Venn, A. A. *et al.* Impact of seawater acidification on pH at the tissue–skeleton interface and calcification in reef corals. *Proc. Natl Acad. Sci. USA* **110**, 1634–1639 (2013).
14. Fantazzini, P. *et al.* A time-domain nuclear magnetic resonance study of Mediterranean scleractinian corals reveals skeletal-porosity sensitivity to environmental changes. *Environ. Sci. Technol.* **47**, 12679–12686 (2013).
15. Ries, J. B., Cohen, A. L. & McCorkle, D. C. Marine calcifiers exhibit mixed responses to CO_2-induced ocean acidification. *Geology* **37**, 1131–1134 (2009).
16. McCandless, E. L. & Craigie, J. S. Sulfated polysaccharides in red and brown algae. *Ann. Rev. Plant Physiol.* **30**, 41–53 (1979).
17. Mann, S., Webb, J. & Williams, R. J. P. *Biomineralization: Chemical and Biochemical Perspectives* (VCH Verlagsgesellschaft, 1989).
18. Robbins, L. L., Knorr, P. O. & Hallock, P. Response of *Halimeda* to ocean acidification: field and laboratory evidence. *Biogeosci. Discuss.* **6**, 4895–4918 (2009).
19. Kroeker, K. J., Kordas, R. L., Crim, R. N. & Singh, G. G. Meta-analysis reveals negative yet variable effects of ocean acidification on marine organisms. *Ecol. Lett.* **13**, 1419–1434 (2010).
20. Fabry, V. J. Marine calcifiers in a high-CO_2 ocean. *Science* **320**, 1020–1022 (2008).
21. Johnson, V. R., Russell, B. D., Fabricius, K. E., Brownlee, C. & Hall-Spencer, J. M. Temperate and tropical brown macroalgae thrive, despite decalcification, along natural CO_2 gradients. *Glob. Change Biol.* **18**, 2792–2803 (2012).
22. Cornwall, C. E. *et al.* Carbon-use strategies in macroalgae: Differential responses to lowered pH and implications for ocean acidification. *J. Phycol.* **48**, 137–144 (2012).
23. Hofmann, L. C., Straub, S. & Bischof, K. Competition between calcifying and noncalcifying temperate marine macroalgae under elevated CO_2 levels. *Mar. Ecol. Prog. Ser.* **464**, 89–105 (2012).
24. Sarker, M. Y., Bartsch, I., Olischläger, M., Gutow, L. & Wiencke, C. Combined effects of CO_2, temperature, irradiance and time on the physiological performance of *Chondrus crispus* (Rhodophyta). *Bot. Mar.* **56**, 63–74 (2013).
25. Cronin, G. & Hay, M. E. Effects of light and nutrient availability on the growth, secondary chemistry, and resistance to herbivory of two brown seaweeds. *Oikos* **77**, 93–106 (1996).
26. Rohde, S., Hiebenthal, C., Wahl, M., Karez, R. & Bischof, K. Decreased depth distribution of *Fucus vesiculosus* (Phaeophyceae) in the Western Baltic: Effects of light deficiency and epibionts on growth and photosynthesis. *Eur. J. Phycol.* **43**, 143–150 (2008).
27. Munday, P. L., Warner, R. R., Monro, K., Pandolfi, J. M. & Marshall, D. J. Predicting evolutionary responses to climate change in the sea. *Ecol. Lett.* **16**, 1488–1500 (2013).
28. Anderson, J. T., Inouye, D. W., McKinney, A. M., Colautti, R. I. & Mitchell-Olds, T. Phenotypic plasticity and adaptive evolution contribute to advancing flowering phenology in response to climate change. *Proc. R. Soc. B* **279**, 3843–3852 (2012).
29. Dias, B. B., Hart, M. B., Smart, C. W. & Hall-Spencer, J. M. Modern seawater acidification: The response of foraminifera to high-CO_2 conditions in the Mediterranean Sea. *J. Geol. Soc.* **167**, 843–846 (2010).
30. Calosi, P. *et al.* Distribution of sea urchins living near shallow water CO_2 vents is dependent upon species acid-base and ion-regulatory abilities. *Mar. Pollut. Bull.* **73**, 470–484 (2013).

Acknowledgements

Author contributions

S.G., Z.D. and G.F. conceived and designed research. S.G., F.P., E.C. and B.C. collected the samples and performed the diving fieldwork. L.P., S.F., M.R. and G.F. performed the laboratory experiments. S.G., F.P., E.C., B.C., L.P., P.F., M.R., K.E.F. and G.F. analysed the data. All authors wrote the manuscript and participated in the scientific discussion.

Additional information

Supplementary information is available in the online version of the paper. Reprints and permissions information is available online at www.nature.com/reprints. Correspondence and requests for materials should be addressed to S.G. or G.F.

Competing financial interests

The authors declare no competing financial interests.

5